*Geophys. Astrophys. Fluid Dynamics*, Vol. 59, pp. 185–208
Reprints available directly from the publisher
Photocopying permitted by license only



# LINEAR THEORY OF ROTATING FLUIDS USING SPHERICAL HARMONICS PART II, TIME-PERIODIC FLOWS

MICHEL RIEUTORD

*Observatoire Midi-Pyrénées, 14 avenue Edouard Belin, 31400 Toulouse, France and C.E.R.F.A.C.S., 42 avenue Coriolis, 31057 Toulouse, France*

(*Received 3 June 1990; in final form 27 November 1990*)

Expansion in spherical harmonics is used to solve linear equations of flows of homogeneous viscous fluids in a rotating frame. For a truncated series, analytical solutions are obtained for the radial functions. These solutions are used to investigate the modal properties of a viscous incompressible fluid in a spherical shell. The results are compared to the experimental data of Aldridge. The problem of identification of inertial modes in the Earth's outer core is also discussed.

KEY WORDS: Inertial waves, Ekman number, Earth's core.

## 1. INTRODUCTION

In a former paper, Rieutord (1987) (henceforth referred to as I), we presented a new set of solutions for describing steady incompressible flows in a rotating frame at linear approximation. These solutions use expansions in spherical harmonics and apply either to viscous homogeneous fluids or to uniformly stratified viscous fluids (i.e. of constant Brünt–Väisälä frequency). They are well adapted to geometries close to that of the sphere and are thus of natural interest for astrophysical and geophysical problems.

In this paper we pursue the study started in I of the properties of such solutions and we focus particularly on time periodic ones. In the inviscid limit such solutions are inertial modes, the properties of which have been much investigated in the past. We refer the reader to the work of Aldridge who experimentally (Aldridge, 1967; Aldridge and Toomre, 1969) and theoretically (Aldridge, 1972), investigated the properties of the inertial modes of an incompressible fluid in a rotating sphere or spherical shell. These papers give mainly the modal properties of a rotating fluid in a full sphere, while the case of a spherical shell remains largely unknown, despite its importance. The main difficulty in this latter problem, is due to the fact that no analytical solution is known for the inviscid problem (zeroth order in the boundary layer theory). In addition, it is an ill-posed boundary value problem (see Stewartson and Rickard, 1969; Aldridge, 1972) therefore very few results are available from mathematical analysis. The approach we use allows us to include viscosity, making the problem well posed and tractable.

The aim of this paper is twofold: first we wish to present the wide possibilities of applications of expansions in spherical harmonics to problems of rotating fluids and second to bring some new light on the problem of modal properties of a fluid in a rotating spherical shell and especially its application to the Earth's outer core.

After recalling briefly the set of equations that are solved and the expression of solutions in series of spherical harmonics (Section 2), we compare these solutions to experimental data obtained by Aldridge (1967) and we also study the influence of the core on the inertial modes (Section 3). Then the recent problem of identification of inertial waves in the Earth's outer core is discussed briefly (Section 4).

## 2. THE FORMALISM

### *2.1 Equations*

If we consider a homogeneous incompressible fluid in a rotating shell, equations for perturbations can be written in dimensionless form as

$$\begin{aligned} \partial \mathbf{u}/\partial \tau + \mathbf{e}_z \times \mathbf{u} &= -\nabla P + E\Delta \mathbf{u}, \\ \nabla \cdot \mathbf{u} &= 0, \end{aligned} \tag{1}$$

or, eliminating the pressure, as

$$\begin{aligned} \nabla \times (\partial \mathbf{u}/\partial \tau + \mathbf{e}_z \times \mathbf{u}) &= E\Delta \nabla \mathbf{u}, \\ \nabla \cdot \mathbf{u} &= 0, \end{aligned} \tag{2}$$

where the time scale and length scale are respectively $(2\Omega)^{-1}$ and $R$; $\Omega$ being the angular velocity of the shell and $R$ the radius of the outer shell. The dimensionless number $E$ is the Ekman number

$$E = \nu/2\Omega R^2, \tag{3}$$

where $\nu$ is the kinematic viscosity. These equations are completed by the boundary conditions specific of the problem. In the following applications we shall always use the rigid (noslip) boundary conditions.

To solve this system we expand the fields (velocity $\mathbf{u}$ and pressure $P$) into spherical harmonics, in the form*

$$\mathbf{u} = u_m^l \mathbf{R}_l^m + v_m^l \mathbf{S}_l^m + w_m^l \mathbf{T}_l^m, \quad P = p_m^l Y_l^m, \tag{4}$$

with

$$\mathbf{R}_l^m = Y_l^m \mathbf{e}_r, \quad \mathbf{S}_l^m = \nabla Y_l^m, \quad \mathbf{T}_l^m = \nabla \times \mathbf{R}_l^m, \tag{5}$$

*We assume summation on repeated indices. The top or bottom place of the indices has only aesthetic meaning.

where $Y_l^m$ are the standard normalized spherical harmonics, $\mathbf{e}_r$ is the unit radial vector and $\mathbf{V}$ is taken on the unit sphere.

If such an expansion is used in (2) the partial differential equations yield the set of partial differential equations for the radial functions $u_m^l, v_m^l, w_m^l$

$$E\Delta_l w_m^l + \left[\frac{im}{l(l+1)} - \frac{\partial}{\partial\tau}\right] w_m^l = -A_{l-1}^l x^{l-1} \frac{\partial}{\partial x}\left(\frac{u_m^{l-1}}{x^{l-2}}\right) - A_{l+1}^l x^{-l-2} \frac{\partial}{\partial x}(x^{l+3} u_m^{l+1}),$$

$$E\Delta_l \Delta_l (x u_m^l) + \left[\frac{im}{l(l+1)} - \frac{\partial}{\partial\tau}\right] \Delta_l (x u_m^l) \tag{6}$$

$$= B_{l-1}^l x^{l-1} \frac{\partial}{\partial x}\left(\frac{w_m^{l-1}}{x^{l-1}}\right) + B_{l+1}^l x^{-l-2} \frac{\partial}{\partial x}(x^{l+2} w_m^{l+1}),$$

$$l(l+1) v_m^l = \frac{1}{x} \frac{\partial}{\partial x}(x^2 u_m^l),$$

where

$$A_{l-1}^l = A_l^{l-1} = \frac{1}{l^2}\sqrt{\frac{l^2-m^2}{4l^2-1}},$$

$$B_{l-1}^l = B_l^{l-1} = (l^2-1)\sqrt{\frac{l^2-m^2}{4l^2-1}}, \tag{7}$$

and $x$ is the dimensionless radial coordinate.

### 2.2 *Solutions*

We shall look for time periodic solutions so that all functions will be taken proportional to $\exp(i\gamma t)$. In order to solve this system we shall truncate the expansion in spherical harmonics to a finite order ($L_{\max}$) so that all the radial functions with $l > L_{\max}$ are set to zero. Then the set of equations (6), truncated to a finite order $L_{\max}$, admit exact solutions in terms of polynomials or Bessel type functions. These solutions may be written

$$u_m^l = \sum_{i=1}^{i_{\max}} V_m^{l,i} [A_m^i j_l(\mu_m^i x)/\mu_m^i x + B_m^i y_l(\mu_m^i x)/\mu_m^i x]$$

$$+ \sum_{j=m,m+2,\ldots} C_m^j P_m^{l,j}(x) + D_m^j Q_m^{l,j}(x^{-1}),$$

$$v_m^l = l^{-1}(l+1)^{-1} x^{-1} \partial(x^2 u_m^l)/\partial x, \tag{8}$$

$$w_m^l = \sum_{i=1}^{i_{\max}} V_m^{l,i}[A_m^i j_l(\mu_m^i x) + B_m^i y_l(\mu_m^i x)]$$

$$+ \sum_{j=m,m+2,\ldots} C_m^j P_m^{l,j}(x) + D_m^j Q_m^{l,j}(x^{-1}),$$

where $i_{\max} = \min(L_{\max} - |m| + 1, L_{\max})$ is the number of eigenvalues, $j_l$ and $y_l$ are spherical Bessel functions of the first and second kinds, $\mu_m^i$ and $V_m^{l,i}$ are the eigenvalues and eigenvectors of the matrix derived from (6) when Bessel functions are substituted (see Appendix). The $P_m^{l,j}$ and $Q_m^{l,j}$ are polynomials. The constants $A_m^i, B_m^i, C_m^i$ and $D_m^i$ are determined by the boundary conditions of the problem. The pressure may be obtained from (1) as

$$p_0^0(x) = \frac{2}{\sqrt{3}} \left\{ -\sum_i W_1^i [A^i j_0(\mu_i x)/\mu_i + B^i y_0(\mu_i x)/\mu_i] \right.$$

$$\left. + \sum_j C_j \int P_1^j(x)\,dx + D_j \int Q_1^j(x^{-1})\,dx \right\}, \tag{9}$$

$$p_m^l = l^{-1}(l+1)^{-1}\{E\partial[x\Delta_l(xu_m^l)]/\partial x + imx(u_m^l + v_m^l)\} + i\gamma x v_m^l$$

$$-(l-1)lA_{l-1}^l x w_m^{l-1} - (l+1)(l+2)A_{l+1}^l x w_m^{l+1}, \qquad l \neq 0.$$

We have given all the technical details of this method (in particular how to compute the eigenvalues $\mu_m^i$ and the polynomials) in the Appendix.

As as a general remark let us note that these solutions preserve the separation between interior almost inviscid solutions (the polynomials) and boundary layer solutions (the Bessel functions). This separation allows much simplification in the case of small Ekman numbers since results from the boundary layer theory can be used.

Then, it should be pointed out that the polynomials $P_m^j$ are exact solutions of (6) (see Appendix), or that

$$\mathbf{u}_m^j = \sum_{l=m}^{j} P_m^{l,j}(x)\mathbf{R}_l^m + P_m'^{l,j}(x)\mathbf{S}_l^m + P_m^{l,j}(x)\mathbf{T}_l^m, \tag{10}$$

where $P_m'^{l,j}(x) = l^{-1}(l+1)^{-1}x^{-1}\partial[x^2 P_m^{l,j}(x)]/\partial x$, is an exact solution of (2). Such solutions, of course, do not meet any (realistic) boundary conditions at the surface of the sphere. However, when the viscosity is zero* they can be combined to meet the boundary conditions of the inviscid fluids ($\mathbf{u}\cdot\mathbf{e}_r = 0$); this combination then

*The polynomials $P$ and $Q$ are the only solutions to survive when viscosity is set to zero.

describes the inertial modes of the cavity. The eigenfrequency of these modes can be computed both for the full sphere and the spherical shell. For the full sphere, the eigenfrequencies given by Greenspan (1969) are found again. For the spherical shell, this frequency depends on the radius of the inner core.

For instance, we computed this frequency for the first axisymmetric mode [(4,1) in Greenspan's notation] when the radius of the inner core is small. Using an expansion with 4 spherical harmonics, we found:

$$\gamma = \sqrt{3/7}[1-(5/7)\eta^5] + O(\eta^7) \tag{11}$$

This dependence in $\eta^5$ at lowest order shows that large scale modes are quite insensitive to the presence or absence of an inner core. In the case of the Earth ($\eta = 0.4$) such shift in frequency is less than one percent. This result however is not true for modes of higher order as can be noticed from Figures 1, 2, 3. There we plotted the pressure response (measured as the pressure difference between the poles of the inner and outer sphere) for different inner radii ($\eta = 0$, $\eta = 0.4$, $\eta = 0.8$) and for an excitation of the fluid similar to that used in the Aldridge experiment (see below). On these spectra one can identify the main modes $(n, 1)$ and the viscous break off at low frequencies. The geostrophic mode which would be resonant at $\gamma = 0$, appears as a little peak around $\gamma = 0.075$ (for $\eta = 0$) because of the form of the excitation (see 18). One can note from the curves $\eta = 0$ and $\eta = 0.4$, that only the modes (4,1) and (6,1) keep their frequency close enough to be identified. However, as shown by Figures 4 and 5 the spatial structure is seriously modified by the presence of the inner core.

### *2.3 Convergence of the Series*

An important question to address before concluding this section, is that of the convergence of the spherical harmonic series.

To see how fast the series converge towards the solutions, we plotted in Figure 6 the relative difference between two values of $C_p$ (the quantity plotted in Figure 9) computed with $L_{\max}$ and $L_{\max}+2$ spherical harmonics. We repeated this computation for different values of the Ekman number.

The curves show that for Ekman numbers larger than $10^{-2}$, the convergence rate is extremely fast and very few spherical harmonics suffice to describe the solution accurately. The reason is that the rotation is moderate and the property of the non-rotating solutions that spherical harmonics components are all decoupled, is already felt. The decrease of the spherical components is then almost exponential. For lower Ekman numbers, the convergence is not so fast and becomes algebraic when the asymptotic solution ($E = 0$) is reached (that is $E < 10^{-10}$). Because of its importance in applications, we shall now look closer at the expansion in spherical harmonics of an asympotic solution.

For the sake of simplicity, let us consider the steady spin-up flow in a full sphere, which was already used in I. The leading component of the flow is a geostrophic flow (see (3.4) in I) which reads

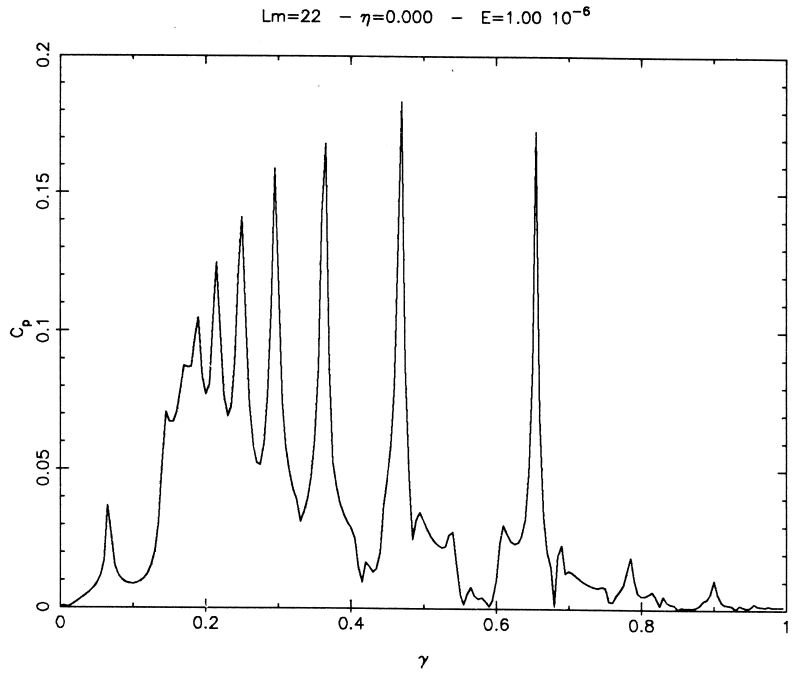


**Figure 1** Pressure response measured at the North pole of the external sphere. The sphere is full ($\eta = 0$), the Ekman number is $10^{-6}$ and the series were truncated at $L_{max} = 22$.

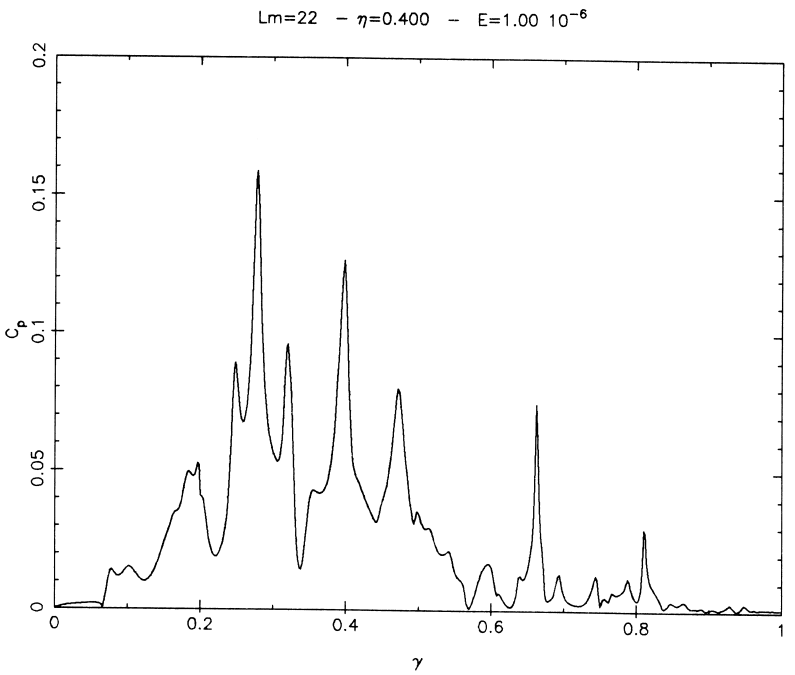


**Figure 2** As Figure 1 but with $\eta = 0.4$.

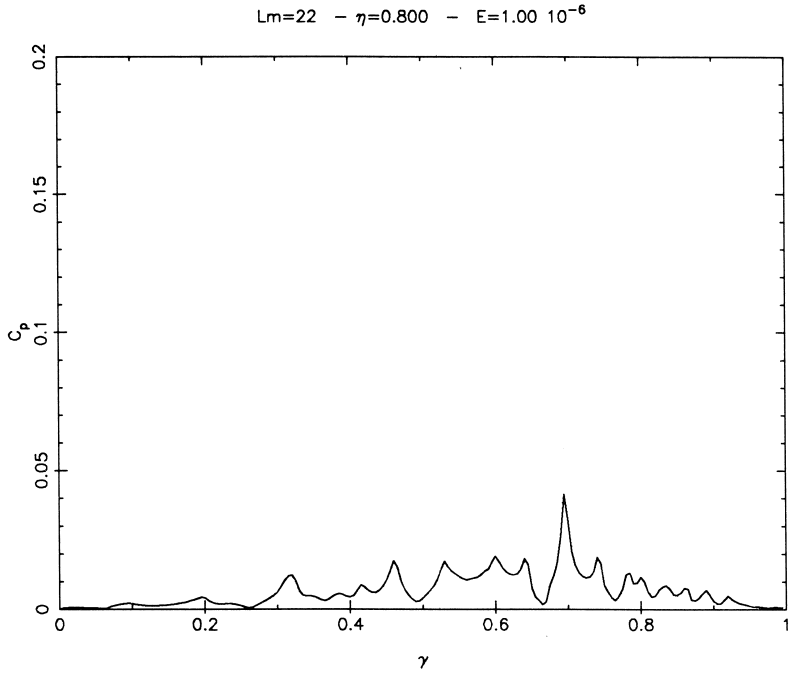


**Figure 3** As Figure 1 but with $\eta = 0.8$.

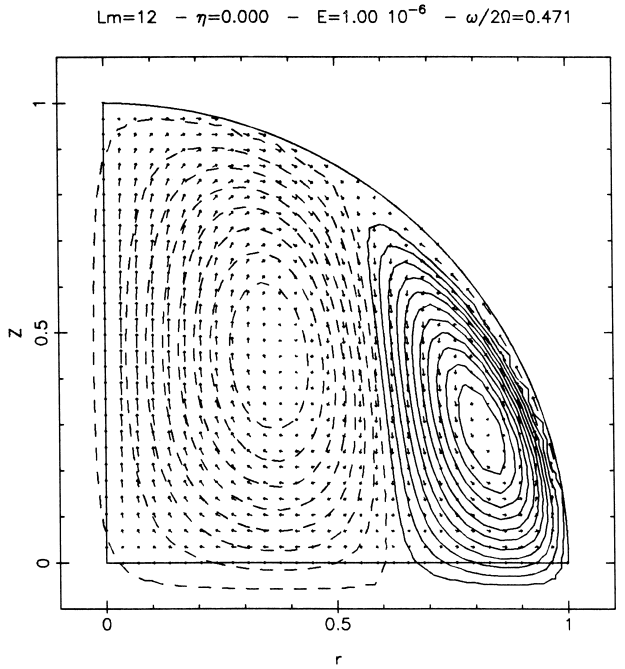


**Figure 4** Meridional section of the flow for the full sphere when the (6, 1) mode is excited ($\omega/2\Omega = 0.471$). The Ekman number is $10^{-6}$ and $L_{max} = 12$ (Note that a defect of the contour plot program makes the streamlines rather bad close to the sides of the container).

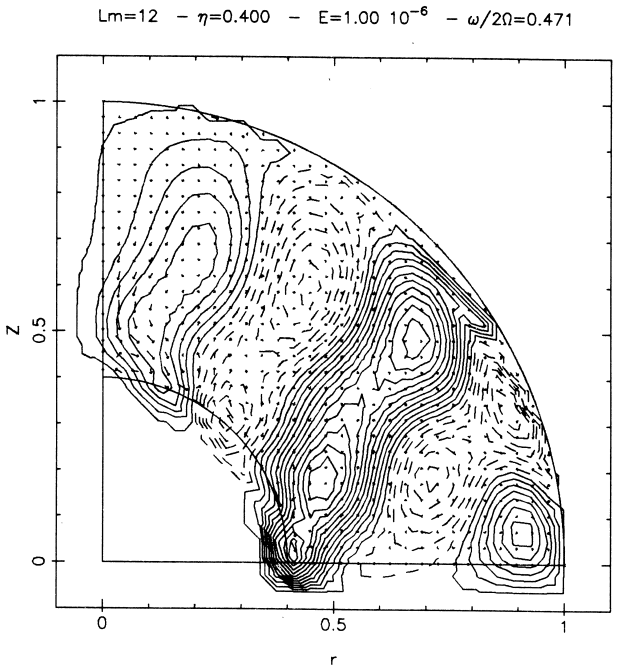


**Figure 5** As Figure 4 but with $\eta = 0.4$.

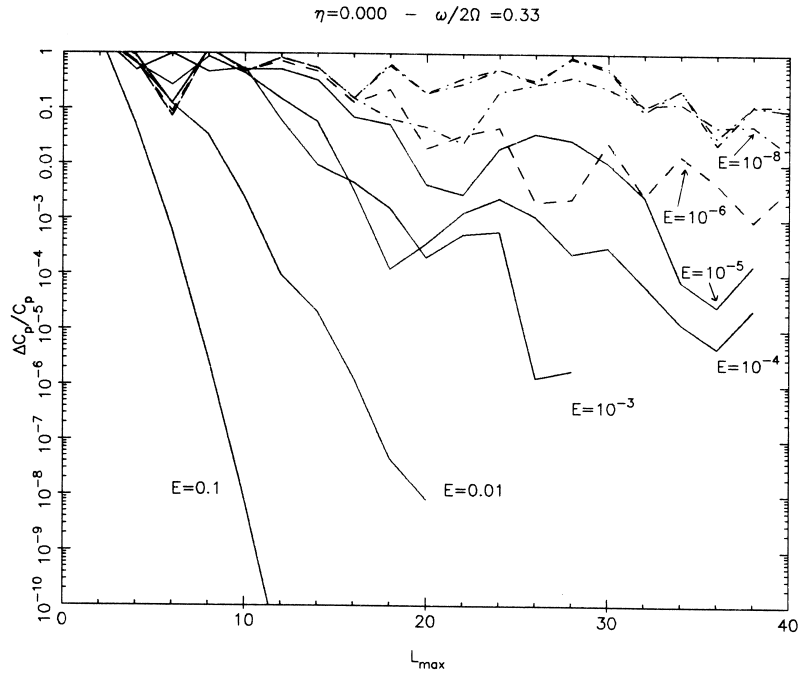


**Figure 6** The rate of convergence of the spherical harmonics series for one point of Figure 9 ($\Omega/\omega = 1.5$), but for several values of the Ekman number. The two very close and not annotated curves on the top of the figure were computed with $E = 10^{-10}$ and $10^{-12}$.

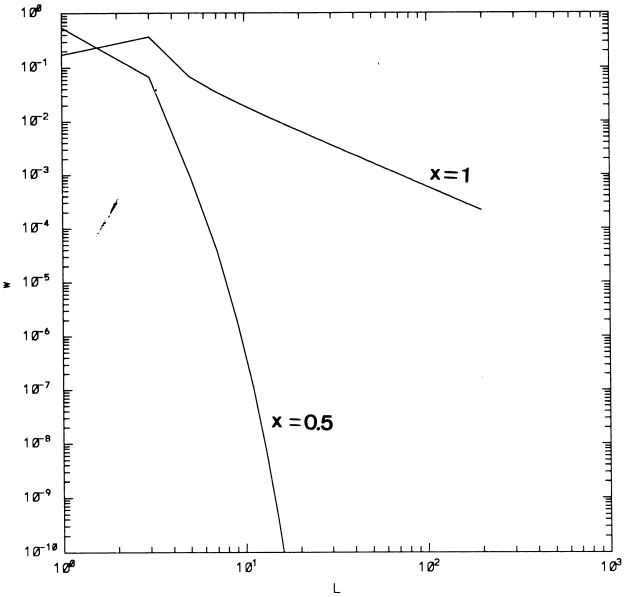


**Figure 7** The radial functions $w^l$ for the asymptotic solution (3.4) of the paper I as a function of $l$, at two different locations $x=0.5$ and $x=1$.

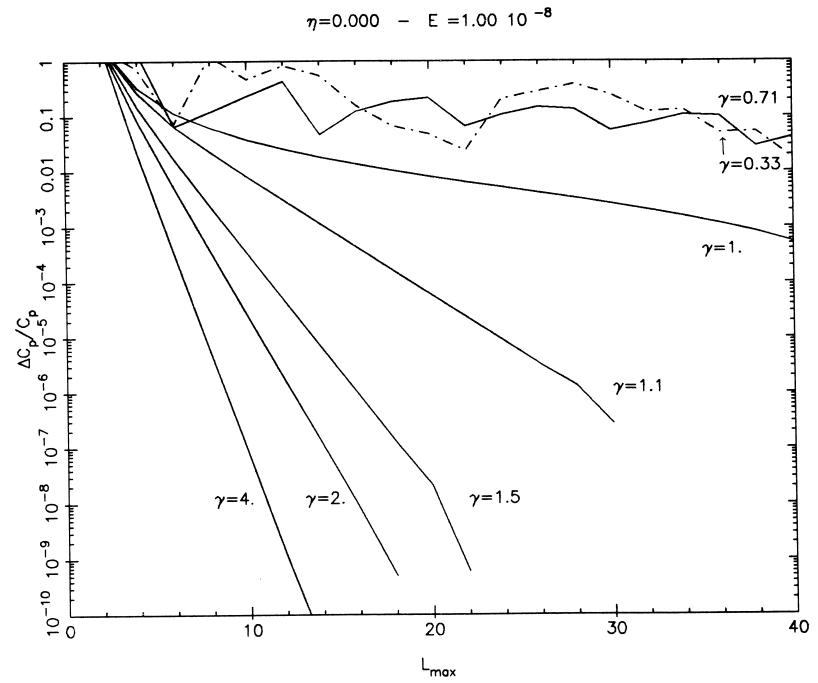


**Figure 8** As Figure 6 but for a fixed value of the Ekman number ($E=10^{-8}$) and several values of $\gamma$.

$$\mathbf{u}=\frac{x\sin\theta}{\sqrt{E}}\alpha^3\{[1-(\cos\alpha\zeta)e^{-\alpha\zeta}]\mathbf{e}_\phi-(\sin\alpha\zeta)e^{-\alpha\zeta}\mathbf{e}_\theta\}, \tag{12}$$

when completed by its boundary layer counterpart, $\alpha=(1-x^2\sin^2\theta)^{-1/4}$ and $\zeta=(1-x)/\sqrt{E}$. The decomposition of this solution in spherical harmonics is quite instructive. The radial functions $w_0^l(x)$ may be obtained from

$$l(l+1)w_0^l(x)=-\int_{4\pi}u_\phi\frac{\partial Y_l^0}{\partial\theta}d\Omega, \tag{13}$$

which may be expressed as

$$l(l+1)w_0^l(x)=\frac{8\pi x}{\sqrt{E}}\int_0^{\pi/2}\frac{\cos\theta(1-(7x^2/4)\sin^2\theta)}{(1-x^2\sin^2\theta^2\theta)^{1/4}}Y_l^0\sin\theta\,d\theta, \tag{14}$$

in the interior ($x<1$), and as

$$l(l+1)w_0^l(x)=\sqrt{\frac{4\pi}{3}}\frac{2(1-x)}{5E}\left(\delta_{l1}+\sqrt{\frac{3}{7}}\delta_{l3}\right), \tag{15}$$

in the boundary layer ($1-x\ll\sqrt{E}$) where $\delta_{ij}$ is the Kronecker symbol. This last expression shows that the boundary layer flow is very well described by the spherical harmonics series. The inviscid part is, on the other hand, not so well represented. To evaluate the convergence of the series, we plotted in Figure 7 the integral

$$I_l=-4\int_0^1\frac{z[1-7x^2(1-z^2)/4]}{[1-x^2(1-z^2)]^{1/4}}Y_l^0(z)\,dz$$

as a function of $l$ for two different locations in the interior. The first location is at mid-radius ($x=0.5$) and is typical of the main part of the interior flow; at all values of $x$ not close to unity, the series converges rapidly. The value $x=1$ (second curve) is in fact the part of the solution which is worse represented by spherical harmonics. This is so because

$$I_l(1)=\int_0^1\sqrt{z}(3-7z^2)Y_l^0(z)dz, \tag{16}$$

goes to zero as $l^{-3/2}$. This part of the solution unfortunately plays an important role in the final solution. It is indeed in the region of asymptotic matching between the interior solution and the boundary layer one, i.e. when

$$\sqrt{E}\ll 1-x\ll 1, \tag{17}$$

so its misrepresentation by spherical harmonics is affecting the whole interior flow.

The dependence of the convergence rate with the frequency is also interesting. As is shown by Figure 8, convergence is faster with increasing frequency. This picture also clearly shows the separation between the hyperbolic solutions ($\gamma < 1$) and the elliptic ones ($\gamma > 1$). For these latter solutions the influence of rotation is small and fast convergence is recovered.

Finally let us mention the problem of the singular regions of the boundary layer near the critical latitude [$\lambda_{crit} = \sin^{-1}(\omega/2\Omega)$]. Previous investigations [e.g. Friedlander (1976)] have concluded that this region did not play any dynamical role. This implies that such region is affecting the convergence rate only locally in a vanishingly small part of the flow (see I also). This is the opposite of the asymptotic matching region which imposes its convergence rate on almost the whole flow.

The results above have been derived from the special example of the steady spin-up, but are in fact of more general relevance. The slow convergence of the series causes difficulties only at very low $E$; Figure 6 shows that for $E \geqq 10^{-6}$ the series still converge rather rapidly and so leave many applications possible. At lower Ekman number, a possible way to accelerate the convergence of the series is to remove the $\sqrt{|\cos\theta|}$ dependency from the solution; this is however yet to be implemented.

## 3. THEORY VERSUS EXPERIMENT

The final test of any theoretical model is certainly its confrontation with experiment. Such a confrontation is here provided by the experiments of Aldridge (1967). The experimental set up is described in Aldridge and Toomre (1969). We recall here that axisymmetric inertial modes were excited by giving a sinusoidal rotation of the form

$$\Omega(t) = \Omega_0 + \varepsilon\omega\cos(\omega t), \tag{18}$$

to a sphere (or spherical shell) filled with water ($\Omega_0$ is a constant and $\varepsilon \ll 1$). The response of the fluid was measured through the pressure response at a point on the axis of rotation. To obtain the theoretical counterpart of the experimental results we have to solve (1) with the forcing corresponding to (18). After linearisation (keeping terms of first order in $\varepsilon$) and adimensionalization, the equations of the flow are

$$\begin{aligned} i\gamma\mathbf{u} + \mathbf{e}_z \times \mathbf{u} &= -\nabla P + E\Delta\mathbf{u} - \tfrac{1}{2}\mathbf{e}_z \times \mathbf{x}, \\ \nabla \cdot \mathbf{u} &= 0, \end{aligned} \tag{19}$$

where $E = \nu/(2\Omega_0 R^2)$. The term $\frac{1}{2}\mathbf{e}_z \times \mathbf{x}$ is the forcing due to the acceleration of the angular velocity of the frame. The boundary conditions are rigid $\mathbf{u} = 0$ on the inner

and outer spheres. In Figures 9 to 13 we reproduce the experimental data along our theoretical predictions based on solutions (8).

We see that agreement is quite good, especially for the full sphere. Experimental amplitudes are however, systematically lower than the theoretical ones. This discrepancy (around 15 percent) is certainly the effect of nonlinear terms.

In Table 1 we present the damping rates of the modes computed with these solutions, together with their experimental counterpart and the previous boundary layer analysis of Greenspan (1969). These numbers show that expansions in spherical harmonics give a better agreement with experimental data than boundary layer theory. The reason is that the viscous coupling between modes is better accounted for with these solutions than with boundary layer theory.

## 4. THE EARTH'S OUTER CORE

One of the major fields of application of the modal properties of a rotating fluid in a spherical shell, is obviously the Earth's outer core. This subject enjoyed recent interesting developments when Aldridge and Lumb (1987) (hence referred to as AL87) noticed that the long period gravimetric data of Melchior and Ducarme (1986) might be exhibiting the presence of inertial waves in the core.* However, a major problem for identifying core inertial modes in the data is that the core response is very much unknown theoretically (see Melchior *et al.*, 1988; Aldridge *et al.*, 1988, 1989; Lumb and Aldridge, 1988; Gunn and Aldridge, 1988). At the moment the principal effects that have not been accounted for are the presence of the core and the stratification.

In Figure 14, we plotted the response of the fluid in a spherical shell with $\eta = 0.4$ (as the core of the Earth), when inertial modes of $0^+$ symmetry† are excited through a mechanism similar to that of the Aldridge experiment (see above). We selected in the spectral response the period interval of 12 hours to 20 hours and plotted along the response of the shell, the observed periods of Melchior and Ducarme (1986), as reported by AL87. For comparison we plotted in Figure 15 the same data with the response of a full sphere.

The coincidence of observed periods and predicted ones is not quite convincing. The reason may be that other types of symmetry are excited. We thus investigated two other symmetries: $1^+$ and $1^-$. In Figure 16, we plotted the pressure perturbation at the equator when the inner core oscillates along the $x$-axis thus exciting the inertial waves $1^+$. Figure 17 shows the spectrum of inertial waves with $1^-$ symmetry. Such waves can be excited when the core oscillates around the $y$-axis in the following way

$$\mathbf{\Omega}_{\text{core}} = \mathbf{\Omega}_0 \mathbf{e}_z + \varepsilon\omega \cos \omega t \mathbf{e}_y. \tag{20}$$

*This discovery is however controversial see Zürn *et al.* (1987).

†We classify the inertial modes according to their symmetry which is referred to by a symbol $m^+$ or $m^-$ which refers to the azimuthal dependence $\exp(im\phi)$ and its symmetry $(+)$ or antisymmetry $(-)$ with respect to equator.

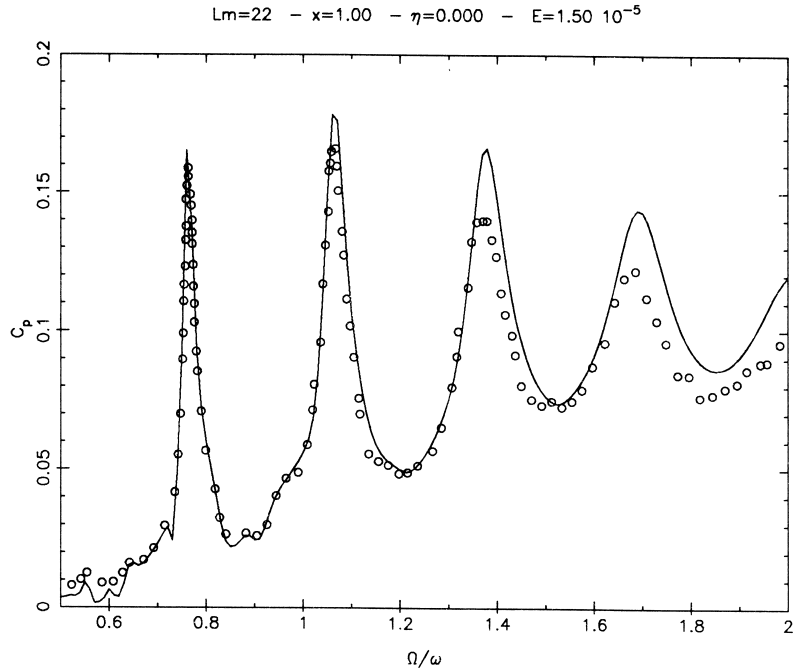


**Figure 9** Pressure response of a fluid in a full sphere along experimental data of Aldridge. Measurement is taken at the North pole of the sphere ($x=1$). For the definition of $C_p$ see Aldridge and Toomre (1969). $L_{max}=22$.

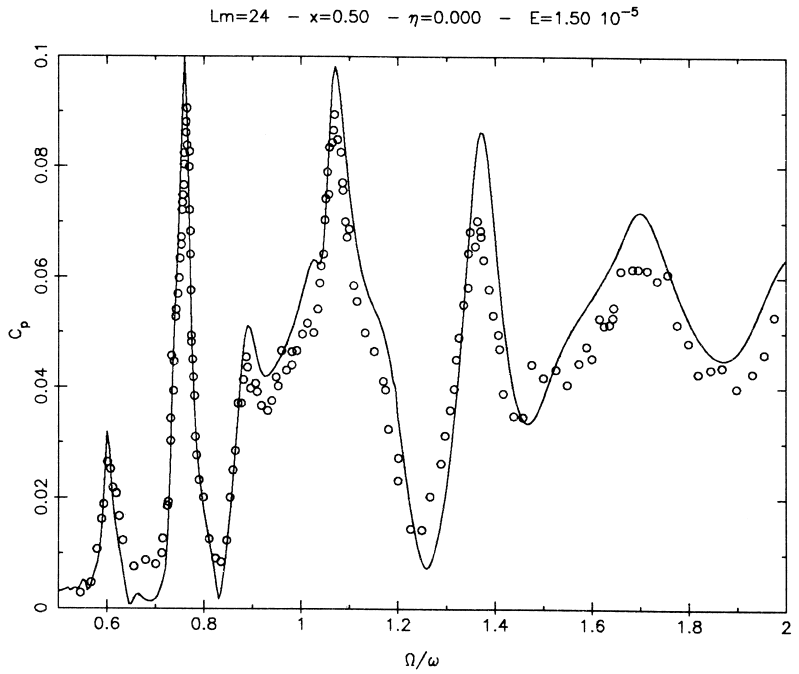


**Figure 10** As Figure 6 but measurement is done at $x=0.5$ ($L$max $=24$).

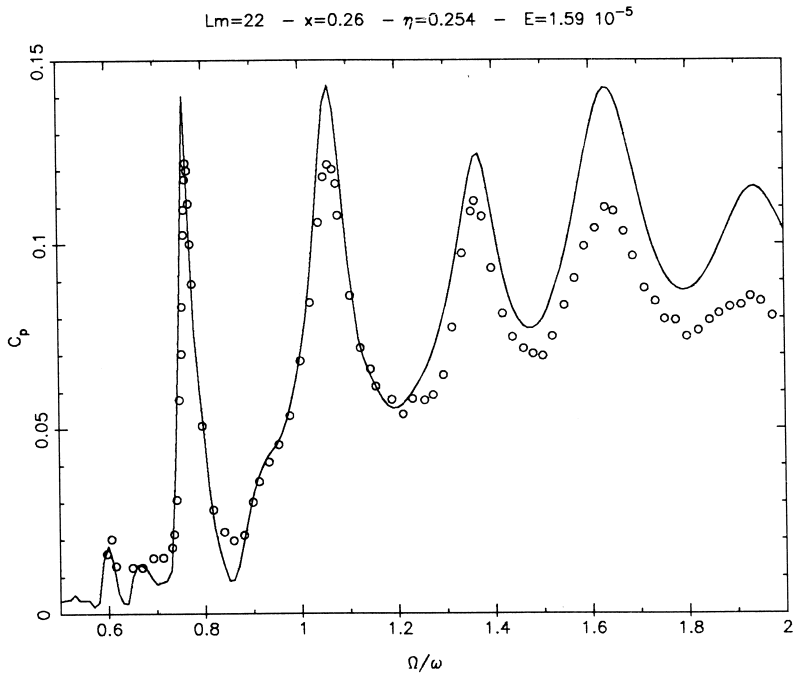


**Figure 11** As Figure 6 but for a shell with $\eta = 0.254$ and measurement $x = 0.26$ ($L_{max} = 22$).

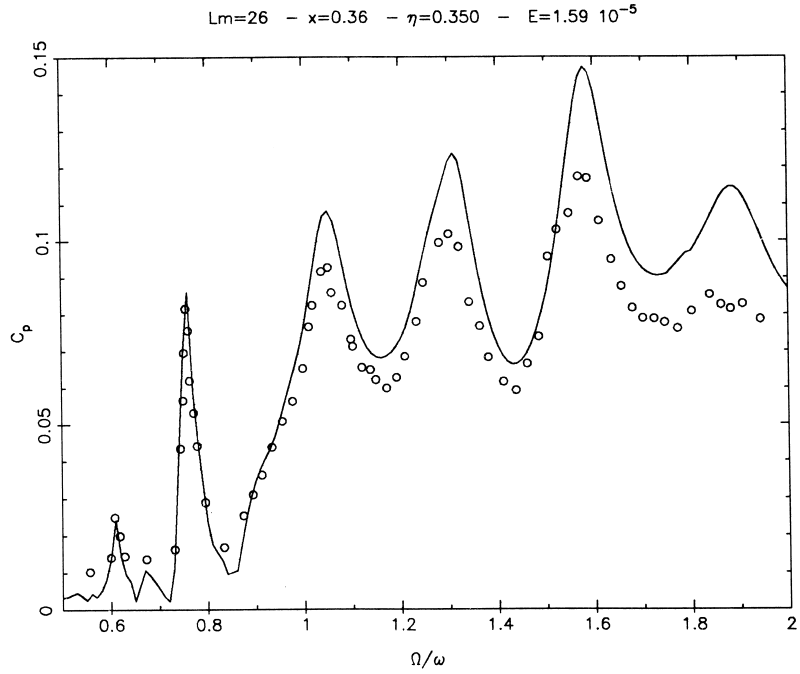


**Figure 12** As Figure 8 but with $\eta = 0.349$ and $x = 0.36$ ($L_{max} = 26$).

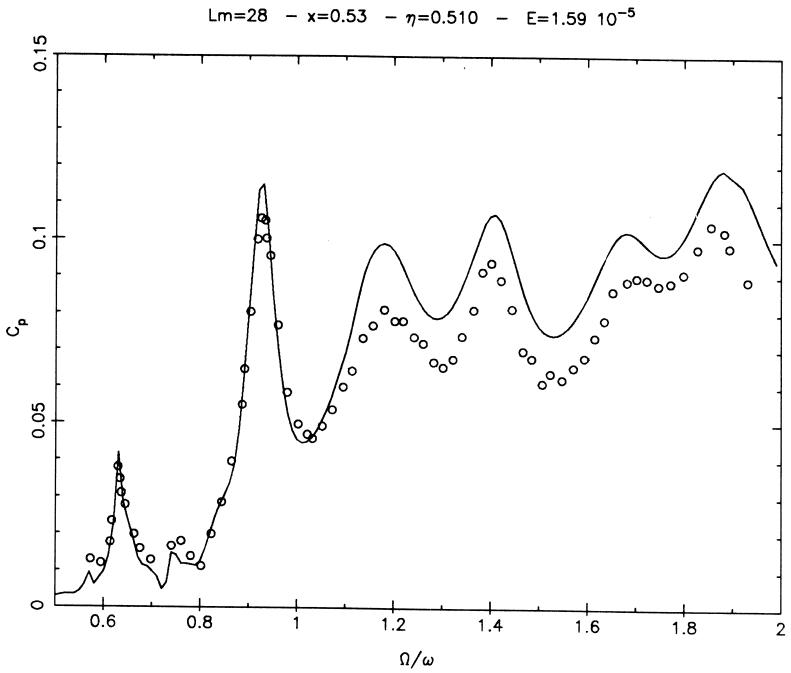


**Figure 13** As Figure 8 but with $\eta = 0.51$ and $x = 0.53$ ($L_{max} = 28$).

**Table 1** Decay factor for the first fundamental axisymmetric inertial modes computed with boundary layer theory (BLT), spherical harmonics decomposition (SH) and from experiment (Exp)

| *Mode* | *Decay factor* | | |
|---|---|---|---|
| | *BLT* | *SH* | *Exp.* |
| (4, 1) | −3.38 | −3.58 | −3.88 |
| (6, 1) | −4.64 | −5.08 | −5.17 |
| (8, 1) | −5.62 | −6.67 | −6.32 |

Its rotation vector has a small component on $\mathbf{e}_y$.

These figures* show that the best coincidence of the observed periods and the peaks of our spectra is achieved by the $1^+$-spectrum. In particular the mode with a period of 15.6 h can be identified. The slight discrepancy on the period (0.4%)

*We have taken for these pictures a very low Ekman number ($10^{-8}$) so that many modes are visible. However, this implies that a large number of spherical harmonics is necessary to achieve accuracy; truncated at $L_{max} \sim 30$, amplitudes are still subject to 10% fluctuations, but the frequency of the resonances, which is the interesting parameter, has already converged.

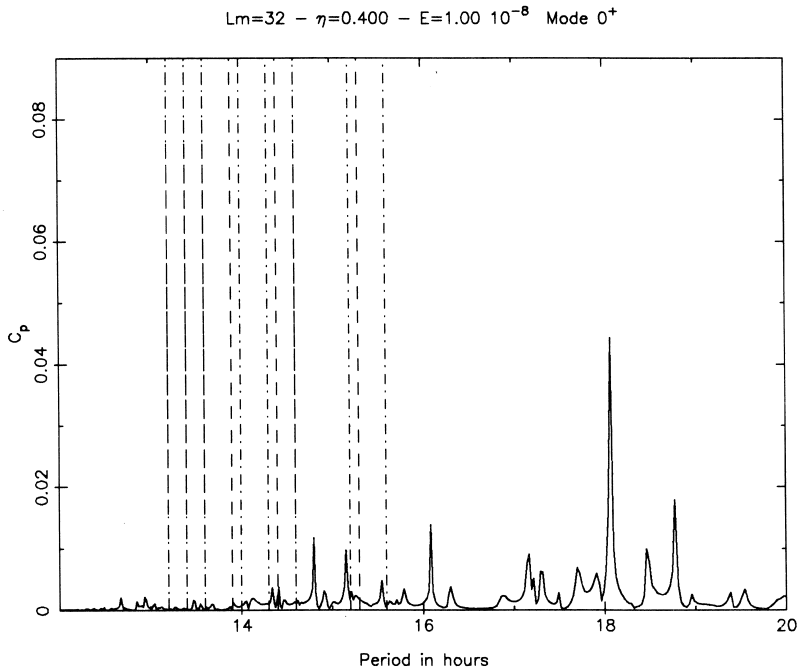


**Figure 14** Spectrum of axisymmetric inertial modes $0^+$ for the $\eta = 0.4$ spherical shell along the observed periods (vertical lines) reported in AL87 ($L_{max} = 32$).

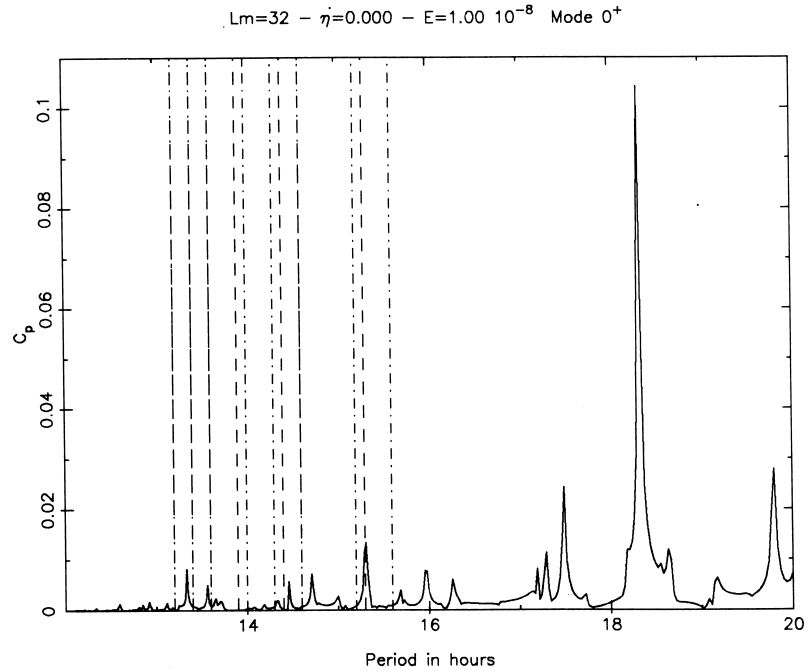


**Figure 15** As Figure 11 but with $\eta = 0$.

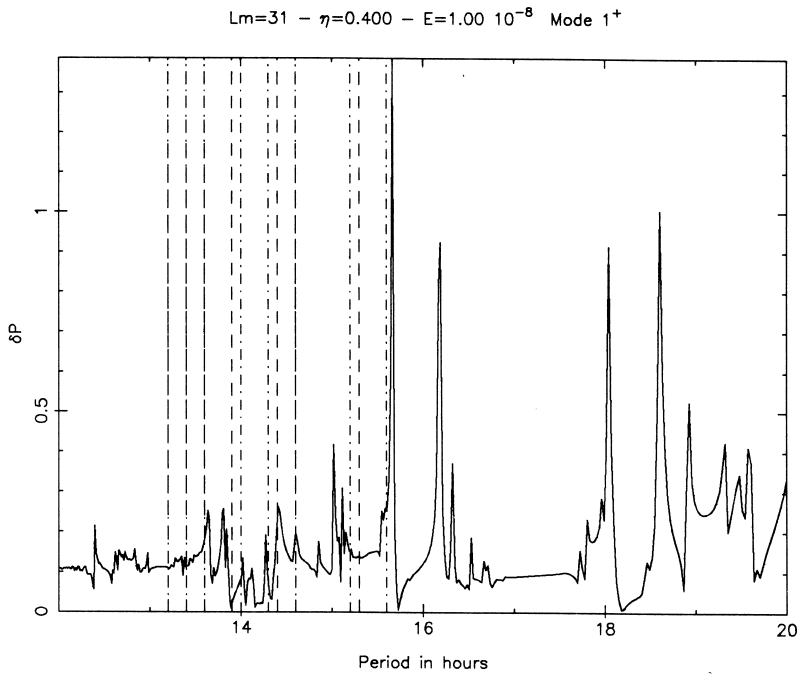


**Figure 16** Spectrum of $1^+$ inertial modes excited by an oscillation of the core along the $x$-axis ($\eta = 0.4$, $L_{max} = 31$).

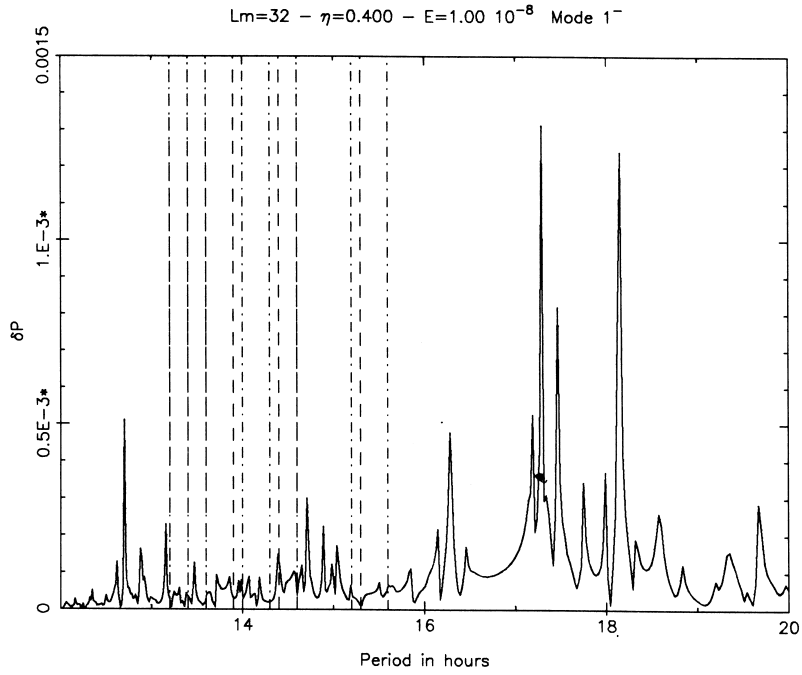


**Figure 17** Spectrum of $1^-$ inertial modes excited by precessing the core ($\eta = 0.4$, $L_{max} = 32$).

could be due to stratification. In total, 5 modes can be identified. This result is certainly encouraging, all the more in that the $1^+$-symmetry is the one likely to be excited by earthquakes happening in the equatorial plane.

Another point of comparison between theory and observation is the width of the resonances, which is directly related to the dissipation mechanism. On this point AL87 noted a serious discrepancy between the decay rate of the modes and the estimated one using Earth's core viscosity. This discrepancy appears also in our results: with an Ekman number of $10^{-8}$ we find a width of resonances which is close to the one observed. However, the value currently accepted for the Earth's core Ekman number is around $10^{-15}$. This means a discrepancy factor of $10^7$ on viscosity. This can be explained if some additional mechanisms of dissipation are operating in the core, like small scale turbulence, non-Newtonian properties of the core's fluid or coupling with magnetic fields.

Our conclusions is that the identification of Earth's core inertial modes in the Melchior and Ducarme data, although not certain, seems to be quite likely. However, more definite conclusions should await the detection of the more intense long period inertial modes. The inclusion of stratification (now under progress) might also provide better agreement. The next step will then be to invert the observations and go back to the physical parameters of the liquid core. For such a purpose our solutions provide an adequate tool.

## 5. CONCLUSIONS

In this paper we have presented some further results on how expansions in spherical harmonics can help us to grasp the physics of rotating fluids in spherical shells. The computation of some time periodic flows and their comparison with experimental data show that this approach is powerful. This power is partly based on the fact that such solutions keep track of the difference between boundary layer and interior solutions and so are good at low Ekman numbers.

What has been presented above is obviously only a sketch of what can be done, however, and much more complex problems can be treated. In an earlier work (Rieutord, 1987b), we used this approach to compute the spin-up of a tidally distorted star. The fluid was treated at the an-elastic approximation, the geometry was a non-axisymmetric ellipsoid with free surfaces.

Concerning the problem of the detection of inertial waves in the Earth's core, we showed that there are indeed some good candidates, but the definite conclusion should await the detection of the modes with the largest amplitudes and the completion of our theoretical understanding of fluid motions in a rotating spherical shell.

*Acknowledgement*

I would very much like to thank Keith Aldridge for letting me know his thesis work and for the enlighting discussions we had together in Cambridge. I thank also a referee for his constructive criticism.

## APPENDIX

We gather here all the technical details of the method presented in the paper.

### *1. Bessel Type Solutions*

If we set

$$u_m^l(x) = -iU^l j_l(\mu x)/\mu x,$$

$$w_m^l(x) = W^l j_l(\mu x),$$

then (6) becomes

$$\begin{aligned} A(l)U^{l-1} + \frac{m}{l(l+1)} W^l - A(l+1)U^{l+1} &= (\lambda+\gamma)W^l, \\ -B(l)W^{l-1} + \frac{m}{l(l+1)} U^l + B(l+1)W^{l+1} &= (\lambda+\gamma)U^l, \end{aligned} \tag{21}$$

with $\lambda = -iE\mu^2$ or $\mu = \sqrt{(i\lambda/E)}$, $i^2 = -1$, $A(l) = A_{l-1}^l = A_l^{l-1}$ and $B(l) = B_{l-1}^l = B_l^{l-1}$. We can write (21) in matrix form

$$\mathbf{MU} = (\lambda+\gamma)\mathbf{U}.$$

One notes that the eigenvectors are independant of $\gamma$ and that $\lambda = \lambda_{\gamma=0} - \gamma$. For a mode $m^-$ $(m \neq 0)$ the matrix $\mathbf{M}$ reads

$$\mathbf{M}^- = \begin{bmatrix} \frac{m}{m(m+1)} & -A(m+1) & 0 & 0 & \cdots \\ -B(m+1) & \frac{m}{(m+1)(m+2)} & B(m+2) & 0 & \cdots \\ 0 & A(m+2) & \frac{m}{(m+2)(m+3)} & \ddots & \\ 0 & 0 & \ddots & \ddots & \ddots \\ \vdots & \vdots & & \ddots & \ddots \end{bmatrix}, \quad \mathbf{U} = \begin{bmatrix} W_m^m \\ U_m^{m+1} \\ W_m^{m+2} \\ \vdots \\ \vdots \end{bmatrix}$$

and for a mode $m^+$ $(m \neq 0)$

$$\mathbf{M}^{+}=\begin{bmatrix} \dfrac{m}{m(m+1)} & B(m+1) & 0 & 0 & \dots \\ A(m+1) & \dfrac{m}{(m+1)(m+2)} & -A(m+2) & 0 & \dots \\ 0 & -B(m+2) & \dfrac{m}{(m+2)(m+3)} & \ddots & \\ 0 & 0 & \ddots & \ddots & \ddots \\ \vdots & \vdots & & \ddots & \ddots \end{bmatrix}, \quad \mathbf{U}=\begin{bmatrix} U_m^m \\ W_m^{m+1} \\ U_m^{m+2} \\ \vdots \\ \vdots \\ \vdots \end{bmatrix}$$

For modes $m=0$, the matrix is obtained from the $m=1$ case by deleting the first line and column and setting the diagonal to zero.
With the correspondance $1^{+} \Rightarrow 0^{-}$, $1^{-} \Rightarrow 0^{+}$.

we have

$$\mathbf{M}(0^{-})=\begin{bmatrix} 0 & B(2) & 0 & 0 & \dots \\ A(2) & 0 & -A(3) & 0 & \dots \\ 0 & -B(3) & 0 & B(4) & \\ 0 & 0 & A(4) & 0 & \\ \vdots & \vdots & & \ddots & \ddots \end{bmatrix} \quad \mathbf{U}=\begin{bmatrix} U_0^1 \\ W_0^2 \\ U_0^3 \\ \vdots \\ \vdots \end{bmatrix}$$

$$\mathbf{M}(0^{+})=\begin{bmatrix} 0 & -A(2) & 0 & 0 & \dots \\ -B(2) & 0 & B(3) & 0 & \dots \\ 0 & A(3) & 0 & -A(4) & \\ 0 & 0 & -B(4) & 0 & \\ \vdots & \vdots & & \ddots & \ddots \end{bmatrix} \quad \mathbf{U}=\begin{bmatrix} W_0^1 \\ U_0^2 \\ W_0^3 \\ \vdots \\ \vdots \end{bmatrix}$$

Truncated to the same order, matrices $\mathbf{M}^{+}$ and $\mathbf{M}^{-}$ have the same set of eigenvalues but the eigenvectors are different.

We give, in Table 2, the first series of eigenvalues (the first line indicates the order $L_{\max}$ of the truncation).

One may notice that the eigenvalues are identical to the dimensionless frequency $\omega/2\Omega$ of the inertial modes in the full sphere. Indeed, they are solutions of the same algebraic equation. This means also that when the excitation frequency gets

**Table 2**

| | | | | | | | | |
|---|---|---|---|---|---|---|---|---|
| $m=0$ | | | | | | | | |
| *1* | *2* | *3* | *4* | *5* | *6* | *7* | *8* | *9* |
| 0.000000 | 0.447214 | 0.000000 | 0.285232 | 0.000000 | 0.209299 | 0.000000 | 0.165279 | 0.00000 |
| | | 0.654654 | 0.765055 | 0.468849 | 0.591700 | 0.363117 | 0.477925 | 0.295758 |
| | | | | 0.830224 | 0.871740 | 0.677186 | 0.738774 | 0.565235 |
| | | | | | | 0.899758 | 0.919534 | 0.784483 |
| | | | | | | | | 0.934001 |
| $m=1$ | | | | | | | | |
| *1* | *2* | *3* | *4* | *5* | *6* | *7* | *8* | |
| 0.500000 | −0.088304 | −0.410004 | −0.591703 | −0.702108 | −0.773611 | −0.822366 | −0.857018 | |
| | 0.754970 | 0.305992 | −0.034095 | −0.268667 | −0.431362 | −0.547035 | −0.631543 | |
| | | 0.854012 | 0.522799 | 0.220227 | −0.018073 | −0.200043 | −0.339105 | |
| | | | 0.902999 | 0.653039 | 0.395126 | 0.171996 | −0.011194 | |
| | | | | 0.930842 | 0.736872 | 0.518892 | 0.316696 | |
| | | | | | 0.948191 | 0.793822 | 0.609050 | |
| | | | | | | 0.959734 | 0.834199 | |
| | | | | | | | 0.967804 | |
| $m=2$ | | | | | | | | |
| *2* | *3* | *4* | *5* | *6* | *7* | *8* | *9* | |
| 0.333333 | −0.115963 | −0.381668 | −0.546284 | −0.654000 | −0.727904 | −0.780644 | −0.819523 | |
| | 0.615963 | 0.233450 | −0.050895 | −0.254997 | −0.402917 | −0.512289 | −0.594914 | |
| | | 0.748218 | 0.442124 | 0.179768 | −0.028855 | −0.192054 | −0.320038 | |
| | | | 0.821722 | 0.576529 | 0.344838 | 0.146202 | −0.018636 | |
| | | | | 0.866986 | 0.667946 | 0.466027 | 0.282672 | |
| | | | | | 0.896892 | 0.732830 | 0.557170 | |
| | | | | | | 0.917705 | 0.780489 | |
| | | | | | | | 0.932779 | |

close to one of these values, one boundary layer solution is transformed into an interior one, since a Bessel function with a small argument is simply a polynomial.

## 2. POLYNOMIAL SOLUTIONS

### *2.1 Solutions Regular at Origin*

We set

$$w_m^l(x)=\sum_k i^{l+k/2+1} q_k^l x^k \equiv P_m^{l,j}(x),$$

$$u_m^l(x)=\sum_k i^{l+k/2+1} q_k^l x^k \equiv P_m^{l,j}(x),$$

where the $q_k^l$ are real quantities. Equations of motion (2) then read

$$\begin{aligned} &A(l)(k-l+2)q_k^{l-1}-\Sigma_l q_k^l - A(l+1)(k+l+3)q_k^{l+1}=E(k-l+2)(k+l+3)q_{k+2}^l, \\ &-\frac{B(l)}{(k+l+2)}q_k^{l-1}+\Sigma_l q_k^l+\frac{B(l+1)}{(k-l+1)}q_k^{l+1}=E(k-l+3)(k+l+4)q_{k+2}^l, \end{aligned} \tag{22}$$

where $\Sigma_l=[m/l(l+1)]-\gamma$.

Each solution is characterized by its order $J$ and its symmetry $m^{\pm}$. To characterize the parity of the solution we shall introduce $i_p$ where $i_p=0$ for $m^+$ solutions and $i_p=1$ for $m^-$ solutions. Then we have

$$J=m+i_p, \quad m+i_p+2,\ldots .$$

The general form of the solutions is

$$f^m=q^m_{J-1}x^{J-1}+\cdots+q^m_{m+1-i_p}x^{m+1-i_p},$$

$$\vdots$$

$$w^{J-3}=q^{J-3}_{J-1}x^{J-1}+q^{J-3}_{J-3}x^{J-3},$$

$$u^{J-2}=q^{J-2}_{J-1}x^{J-1},$$

$$w^{J-1}=q^{J-1}_{J-1}x^{J-1},$$

$$u^J=x^{J-1}.$$

This solution is computed by solving (22) after setting $q^J_{J-1}$ to unity. $f$ stands for $u$ or $w$.

For example: the solution $0^+$, $J=2$ gives

$$w^1=\frac{i}{2}\sqrt{\frac{5}{3}}\frac{x}{\gamma}=P_0^{1,2}(x)$$

$$u^2=x=P_0^{2,2}(x).$$

*2.2 Solutions Regular at Infinity*

In the same way as before we set

$$w^l(x)=\sum_k i^{l+k/2+1}q^l_k x^{-k}\equiv Q^{l,j}_m(x^{-1}),$$

$$u^l(x)=\sum_k i^{l+k/2+1}q^l_k x^{-k}\equiv Q^{l,j}_m(x^{-1}),$$

and obtain

$$A(l)(k+l-2)q^{l-1}_k+\Sigma_l q^l_k+A(l+1)(l-k+3)q^{l+1}_k=E(k+l-2)(k-l-3)q^l_{k-2},$$

$$\frac{B(l)}{(l-k+2)}q^{l-1}_k+\Sigma_l q^l_k+\frac{B(l+1)}{(k+l-1)}q^{l+1}_k=E(k+l-3)(k-l-4)q^l_{k-2}.$$

We notice that these solutions, contrary to those regular at the origin depend on the order of the truncation $L_{\max}$. Their general form is

$$u^J = x^{-J-2},$$

$$w^{J+1} = q^{J+1}_{J+2} x^{-J-2},$$

$$u^{J+2} = q^{J+2}_{J+2} x^{-J-2},$$

$$w^{J+3} = q^{J+3}_{J+2} x^{-J-2} + q^{J+3}_{J+4} x^{-J-4},$$

$$u^{J+4} = q^{J+4}_{J+2} x^{-J-2} + q^{J+4}_{J+4} x^{-J-4},$$

$$\vdots$$

$$f^{L\max} = q^{L_{\max}}_{J+2} x^{-J-2} + \cdots + q^{L_{\max}}_{l_{\max}+i_p} x^{-(L_{\max}+i_p)}.$$

For example: the solution $1^+$, $J=3$, $L_{\max}=3$ gives

$$u^1 = x^{-3} = Q_1^{1,3}(x^{-1}),$$

$$w^2 = q_3^2 x^{-3} = Q_1^{2,3}(x^{-1}),$$

$$u^3 = q_3^3 x^{-3} = Q_1^{3,3}(x^{-1}),$$

with

$$q_3^2 = -\frac{3i}{4\sqrt{5}}(\tfrac{1}{12}-\gamma)\left[\frac{64}{5\times 7\times 9} - -(\gamma-\tfrac{1}{12})(\gamma-\tfrac{1}{6})\right]^{-1},$$

$$q_3^3 = -\frac{6\sqrt{2}}{5\sqrt{7}}\left[\frac{64}{5\times 7\times 9} - (\gamma-\tfrac{1}{12})(\gamma-\tfrac{1}{6})\right]^{-1}.$$

## CORRIGENDUM TO PAPER I

Equation (2.18) should read the same as Eq. (8). The expression given after (2.18) for the pressure field is valid only for $l\neq 0$. Then the expression (3.2) should read

$$xu_0^l(x) = \sum_{i=1}^{2N} A_i U_l^i j_l(\mu_i x') + \sum_{j=2,4,\ldots}^{2N} C_j P_l^j(x') + (4\pi/5)^{1/2}\dot{\omega}x\delta_2^l,$$

$$w_0^l(x) = \sum_{i=1}^{2N} A_i W_l^i j_l(\mu_i x') + \sum_{j=2,4,\ldots}^{2N} C_j P_l^j(x').$$

$m$ should be set to zero in (3.3).

## *References*

Aldridge, K. D., "An experimental study of axisymmetric inertial oscillations of a rotating liquid sphere," Ph.D. Thesis (1967).

Aldridge, K. D., "Axisymmetric inertial oscillations of a fluid in a rotating spherical shell," *Mathematika* **19,** 163–168 (1972).

Aldridge, K. D. and Lumb, I., "Inertial waves identified in the Earth's fluid outer core," *Nature* **325,** 421–423 (1987).

Aldridge, K. D. and Toomre, A., "Axisymmetric inertial oscillations of a fluid in a rotating spherical container," *J. Fluid Mech.* **37,** 306–323 (1969).

Aldridge, K. D., Lumb, I. and Henderson, G., "Inertial modes in the earth's fluid outer core," In: *Structure and Dynamics of Earth's Deep Interior* (Smylie and Hide, eds.). pp. 13–21 (1988).

Aldridge, K. D., Lumb, I. and Henderson, G., "A Poincaré model for the earth's fluid core," *Geophys. and Astrophys. Fluid Dyn.* **48,** 5–23 (1989).

Friedlander, S., "Quasi-steady flow of a rotating stratified fluid in a sphere," *J. Fluid Mech.* **76,** 209 (1976).

Greenspan, H. P., *The Theory of Rotating Fluids.* Cambridge University Press (1969).

Gunn, S. and Aldridge, K. D., "Inertial waves in a differentially rotating fluid," In: *Structure and Dynamics of Earth's Deep Interior* (Smylie and Hide, eds.). pp. 51–53 (1988).

Lumb, I. and Aldridge, K. D., "An experimental study of inertial waves in spheroidal shell of rotating fluid," In: *Structure and Dynamics of Earth's Deep Interior* (Smylie and Hide, eds.). pp. 35–39 (1988).

Melchior, P. J. and Ducarme, B., "Detections of inertial gravity oscillations in the Earth's core with a superconducting gravimeter at Brussels," *Phys. Earth Planet. Int.* **42,** 129–134 (1986).

Melchior, P. J., Crossley, D. J., Dehant, V. P. and Ducarme, B., "Have inertial waves been identified from the earth's core?" In: *Structure and Dynamics of Earth's Deep Interior* (Smylie and Hide, eds.). pp. 1–12 (1988).

Rieutord, M., "Linear theory of rotating fluid, I. Steady flows," *Geophys. and Astrophys. Fluid Dyn.* **39,** 163–182 (1987a).

Rieutord, M., "Tidal heating in close binary stellar system," *Mon. Not. R. Astr. Soc.* **227,** 295–314 (1987b).

Stewartson, K. and Rickard, J. A., "Pathological oscillations of a rotating fluid," *J. Fluid Mech.* **35,** 759–773 (1969).

Zürn, W., Richter, B., Rydelek, P. A. and Neuberg, J., "Detection of inertial gravity oscillations in the earth's core with a superconducting gravimeter at Brussels," *Phys. Earth Planet. Int.* **49,** 176–178 (1987).